From Fractal to Nanorod Porphyrin J-Aggregates. Concentration-Induced Tuning of the Aggregate Size

Norberto Micali,*,† Valentina Villari,† Maria Angela Castriciano,‡ Andrea Romeo,‡ and Luigi Monsù Scolaro*,‡

CNR−Istituto per i Processi Chimico-Fisici, Via La Farina 237, I-98123 Messina, Italy, and Dipartimento di Chimica Inorganica, Chimica Analitica e Chimica Fisica, Università di Messina, Salita Sperone 31, I-98166 Vill. S. Agata, Messina, Italy

Received: February 3, 2006; In Final Form: March 10, 2006

A structural change from fractal to nanorod J-aggregates of tetrakis(4-sulfonatophenyl)porphyrin has been obtained by acting on the intermolecular interaction potential. The size and shape of these self-assembled porphyrin clusters have been monitored under different experimental conditions, by means of polarized and depolarized dynamic light scattering and small and wide angle elastic light scattering. At sufficiently low porphyrin concentration and high ionic strength, the shielded repulsive potential seems to be responsible for the fractal structure of the aggregates. On the contrary, at low ionic strength (nonshielded potential) and high porphyrin concentration, these species self-assemble in a rodlike arrangement. The length of the so-formed rod-shaped aggregates decreases on increasing porphyrin concentration. Moreover, both fractals and rods display a structure-dependent optical activity induced by a chiral template.

Introduction

Self-assembly of molecules, driven by noncovalent intermolecular interactions, is a versatile and convenient route for manufacturing new materials with desired optical and electronic properties.[1−9] To this purpose, tetrapyrrole macrocycles, and porphyrins in particular, are attractive since besides exhibiting the occurrence of strong intermolecular interactions responsible for stacking phenomena, they are electronically and sterically tunable by chemical modification of peripheral substituent groups.[6,10] As a result, a wide variety of self-assembled structures can be obtained, including nanoparticles,[3,11] molecular wires,[4] ordered monolayers,[5] and nanoporous solid materials.[6] Moreover, the close molecular packing in a self-assembled porphyrin aggregate could optimize the electronic coupling, the photon capture, and the delocalization of the excitation energy, which can be exploited for applications in nonlinear optical devices, photoelectric cells, and recording devices and as a model for bacterial light harvesting antenna complexes. The possibility of controlling and tuning either shape or size of the porphyrin clusters is a prerequisite for their use as potential nanodevices.

Moreover, self-assembly mediated by templates allows for obtaining aggregates with additional properties; e.g., chirality can be imposed on the resulting aggregates by using chiral templates.[12−14]

In this respect, the water soluble tetrakis(4-sulfonatophenyl)-porphyrin ($TPPS_4$) has attracted great interest since its diacid form is able to self-aggregate forming extended J-aggregates.[15−26] In these systems, the porphyrins are arranged in a side-by-side geometry and exhibit a very narrow and red-shifted B-band (the so-called J-band). A large variety of experimental conditions, including different inorganic and organic cations,[27,28] polymeric matrixes,[12,29,30] dendrimers,[31,32] surfactants,[33−35] LB films,[36,37] and confined environments,[38−40] have been identified in order to force the formation of these remarkable species. In our previous studies, we have shown that porphyrins are able to form fractal aggregates whose structure is strongly controlled by the properties of the solvent medium[41] and is very sensitive to different initial conditions.[42] In particular, in the case of $TPPS_4$, a combination of light-scattering techniques evidenced the occurrence of structural rearrangements of the fractal clusters depending on the pH and ionic strength.[41] These effects have been explained by taking into account the DLVO (Derjaguin−Landau−Verwey−Overbeek) potential which controls the interactions between particles during the aggregation of colloidal systems. It drives the system to a statistical nucleating aggregate passing through DLCCA (diffusion-limited cluster−cluster aggregation) and DLA (diffusion-limited aggregation) regimes on decreasing pH.[42] On the other hand, the size of the aggregate can be more finely controlled using the confinement within the aqueous core of a microemulsion. We have already shown that these confined aggregates exhibit a rodlike structure and that their transition dipole moments are highly coherent.[38]

A careful survey of the literature about aggregation of the anionic $TPPS_4$ porphyrin shows that some authors found different structural arrangements for the final aggregate,[11,12,26,43] especially regarding structure and size. Our aim is to show how a structural change from fractal to rodlike arrangement can be done in aqueous solutions by simply changing the porphyrin concentration and ionic strength. These parameters, acting on the interaction potential and on the aggregation kinetic rate, lead to final aggregates with different structure and size. The precise knowledge of this behavior is important for achieving a fine-tuning of their optical properties[44−46] and consequently for their potential applications[47−50] or for application of their nanocomposites.[46,51]

* Corresponding authors. Norberto Micali: phone +39 090 2939693, fax +39 090 2939902, e-mail micali@me.cnr.it. Luigi Monsù Scolaro: phone +39 090 6765711, fax +39 090 393756, e-mail lmonsu@unime.it.

† CNR−Istituto per i Processi Chimico-Fisici.

‡ Università di Messina.

10.1021/jp060730e CCC: $33.50
Published on Web 04/05/2006

Experimental Section

Materials. The porphyrin *meso*-tetrakis(4-sulfonatophenyl)-porphyrin tetrasodium salt ($TPPS_4$) was purchased from Aldrich Co. Aqueous stock solutions of this porphyrin were prepared in dust-free Millipore water, stored in the dark, and used within a week from preparation. High purity D- and L-tartaric acid were purchased from Sigma. Samples were prepared by adding porphyrin to tartrate buffer (100 mM) at the selected pH and ionic strength. The pH of the buffer was adjusted to 2.7 by adding NaOH to the solution of tartaric acid. All the measurements have been performed at least 1 h after the addition of porphyrin. In all the cases, the completion of the aggregation process has been checked by following the growth of the 490 nm band (typical for J-aggregated $TPPS_4$) in UV−vis absorption spectra.

For the scattering measurements, the results were not dependent on the chirality of the acid in the buffer and exactly the same correlation functions and intensity profile have been obtained for both the L and D forms.

Setup. Dynamic light scattering (DLS) measurements were performed by using the photon correlation spectroscopy technique: the laser light scattered from the sample was collected, in a selfbeating mode, by means of a R942/02 photomultiplier (cooled at −30 °C) which guarantees less than 10 dark counts/s. A polarized Nd:YAG laser (532 nm) with a power of 20 mW was used for the solution at 3 and 40 μM, whereas a polarized infrared laser diode (780 nm) with a power of 40 mW was used for the more concentrated solutions (250 and 500 μM) to decrease the beam attenuation due to absorption.

To collect the polarized and depolarized contribution to the light scattered from the sample, a Glan-Taylor polarizer was placed in the incident laser path and a Glan-Thomson analyzer was placed in the scattered beam. The signal was sent to a Malvern 4700 submicrometer particle analyzer system to build up the intensity−intensity correlation function $G_2(Q, t) = \langle I(Q, 0)\, I(Q, t)\rangle$, where $|Q| = (4\pi n/\lambda_0)\sin(\theta/2)$ (θ being the scattering angle, n being the refractive index of the solution, and λ_0 being the wavelength of light in a vacuum). For scattered electric fields obeying Gaussian statistics, it follows that $G_2(Q, t) = \langle I\rangle^2 + a|G(Q, t)|^2$ (a being a constant which depends on the experimental setup and $G(Q, t) = \langle E^*(Q, 0)\, E(Q, t)\rangle$ being the scattered electric field autocorrelation function). The angular scanning was performed by using a computerized homemade goniometer.

Artifacts due to fluorescence have been eliminated by setting an interference filter on the observation path during the measurements.

For the static light scattering (SLS) measurements, the scattered intensity of the solvent was subtracted from the intensity angular profiles of the solutions; then, the intensity of toluene was used as a reference to normalize the data. However, the scattering contribution from the buffer is very small in comparison with that from all the solutions.

The static experiments were combined with small angle light scattering (SALS): this optical apparatus performs an optical Fourier transform of the impinging (scattered) wave front on a linear CCD detector (a fibered 1024 element diode array). A 16 bit analog-to-digital converter was employed to digitalize the signal. The intensity scattered by the solvent was taken as the background and subtracted from all the measured spectra.

The temperature was controlled by a homemade water-circulating apparatus which provided a constant value of 298 K with an accuracy of 0.01 K.

After the proper geometrical corrections, SALS data were matched with SLS data by normalization with a secondary standard. However, in the fitting procedure of the intensity profile, a free multiplicative parameter (close to unity) was inserted in order to take into account the unpolarized SALS geometry (see also the following section) and, hence, to improve the matching of the two data sets.

The circular dichroism spectra were recorded on a JASCO 500A spectropolarimeter, equipped with a 450 W xenon lamp. The apparatus was homemade and fully controlled by a PC computer. The ellipticity, θ, was obtained by calibrating the instrument with a 0.06% aqueous solution of D-10-camphorsulfonic acid. The measurements, corrected for the contribution from cell and solvent, were performed at constant temperature ($T = 298 \pm 0.1$ K).

Method. Detailed information on the structure and conformation of aggregates in solution is obtained by measuring both static and dynamic quantities with light scattering. Porphyrin molecules are optically isotropic, but when they aggregate in a J-arrangement, the large interaction between porphyrins (coherence length of the exciton coupling) makes the free displacements of electrons under incident radiation asymmetric, giving rise to optical anisotropy.[38,52] To determine the reorientational motion of an anisotropic particle in solution, all the components of the polarizability tensor, in principle, must be measured. Assuming a cylindrical symmetry of the polarizability tensor, for a dilute solution of monodisperse noninteracting N particles, resulting from the aggregation of small molecules (with respect to the wavelength of radiation), the Rayleigh−Debye−Gans approximation can be used. Thus, the polarized and depolarized field autocorrelation functions in the absence of correlation between translational and rotational motions are[53−55]

$$G_{VV}(\mathbf{Q}, t) = NP(Q)\left[\alpha^2 F_c(Q, t) + \frac{4}{45}\beta^2 F_s(Q, t)F_r(t)\right]$$

$$G_{VH}(\mathbf{Q}, t) = NP(Q)\left[\frac{\beta^2}{15}F_s(Q, t)F_r(t)\right] \qquad (1)$$

where α is the isotropic excess polarizability of the particle with respect to the solvent and β is the anisotropy of the particle polarizability. The structure factor of molecules in the aggregate can be regarded as a form factor $P(Q)$ of the aggregate (particle) itself. The self-intermediate scattering function $F_s(\mathbf{Q}, t) = \langle \exp[i\mathbf{Q}\cdot(\mathbf{r}_j(t) - \mathbf{r}_j(0))]\rangle$ contains information on the translation ($\mathbf{r}_j(t) - \mathbf{r}_j(0)$ being the displacement of particle j at the time t). The collective intermediate scattering function, $F_c(\mathbf{Q}, t)$, in the approximation of a dilute solution coincides with $F_s(\mathbf{Q}, t)$. $F_r(t)$ is a self-rotational correlation function that depends only on the reorientation of a particle and, as a consequence, is purely local in character (independent of Q).

For polydisperse scatterers, the field autocorrelation function may be expressed in terms of the cumulant expansion:[55]

$$\ln\left|\frac{G(Q, t)}{G(Q, 0)}\right| = -\Gamma t + 1/2!\mu_2 t^2 - 1/3!\mu_3 t^3 + \ldots \qquad (2)$$

with μ_n being the moments of the distribution and $\Gamma = -(\mathrm{d}[\ln(G(Q, t))]/\mathrm{d}t)$ at $t = 0$. The CONTIN analysis[56] can also be used to obtain the relaxation rate distribution. In the present case, the distribution is monomodal and the mean relaxation rate is consistent with that obtained by the cumulant expansion.

In Figure 1, some examples of correlation functions are reported along with the fit obtained by the cumulant analysis.

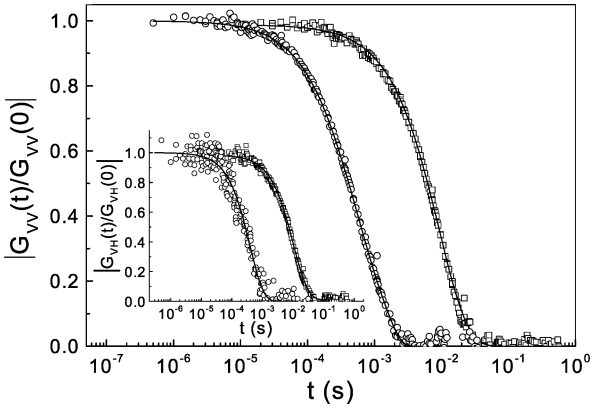

Figure 1. Polarized correlation functions of the solutions at $c_{TPPS} = 3$ μM (squares; in the presence of NaCl) and $c_{TPPS} = 40$ μM (circles), at a scattering angle of 90°. In the inset, the corresponding depolarized correlation functions are reported. The continuous lines are fits according to the second-order cumulant expansion.

The initial decay rate, Γ, of the normalized field correlation functions gives:

$$\Gamma_{VV}(Q) = DQ^2 + \frac{6\Theta}{\frac{45}{4}\frac{\alpha^2}{\beta^2} + 1} \tag{3}$$

$$\Gamma_{VH}(Q) = DQ^2 + 6\Theta \tag{4}$$

where D and Θ are the translational and rotational diffusion coefficients, respectively.

For large particles, the DLS spectrum can contain other information regarding the coupling between translation and rotational motions, so that eqs 3 and 4 are not valid even for dilute solutions. The role of this coupling is taken into account by the coupling parameter[57−59] $\gamma = Q^2\Delta D/\Theta$ (where ΔD is the anisotropy in the translational diffusion motion) which relates rotational and translational correlation times. For small values of γ, the particle can reorient many times before diffusing over a distance close to Q^{-1} and then coupling vanishes.

For rigid spherelike particles, γ is close to zero ($\Delta D = 0$) and eqs 3 and 4 are valid also for large particles. Under this condition, the translation diffusion coefficient is related to the hydrodynamic radius, R_H, through the Einstein−Stokes relation, $D = k_BT/(6\pi\eta R_H)$, and the rotational diffusion coefficient is $\Theta = k_BT/(8\pi\eta R_H^3)$ (k_B being Boltzmann's constant, T being the absolute temperature, and η being the solvent viscosity).

On the other hand, in the case of rigid rod-shaped (or ellipsoidal) particles,[60,61] the rotational and translational diffusions can be correlated. For long particles $QL > 3$ (L being the length of the rod), even in dilute solutions ($NL^3 < 1$), the difference in the lengthways and sideways translational diffusion (ΔD) becomes large and γ plays a important role. For $\gamma < 10$, the DLS spectrum contains up to four exponentials and the initial decay Γ contains also terms in ΔD. However, for $\gamma < 5$, the contribution of these extra terms is less than 10% and eqs 3 and 4 represent a good approximation which well describes the experimental results.

Information on the form factor of the particle can be obtained by static light scattering, which furnishes the isotropic scattered intensity profile:

$$I(\mathbf{Q}) = G_{VV}(\mathbf{Q}, 0) - \frac{4}{3}G_{VH}(\mathbf{Q}, 0) = NP(Q)\alpha^2 \tag{5}$$

In the case of SALS measurements, since the depolarization ratio is less than 10%, the contribution of the depolarized scattering can be neglected at small angles and the intensity can be approximated as $I(\mathbf{Q}) \propto P(Q)$.

Hereafter, some form factors concerning the aggregation of the present system are recalled. For homogeneous spherical particles having a radius R, it is:

$$I(Q) \propto (J_0(QR))^2 \tag{6}$$

where $J_0(QR)$ is the zero-order Bessel function.

For particles possessing a self-similar structure, fractals, for which the spatial correlation density fluctuation is a homogeneous function, the scattered intensity obeys the following power law:[62,63]

$$I(Q) \propto Q^{-D_f} \tag{7}$$

where D_f is the fractal dimension. This scaling law is typical of fractally arranged ideal systems. Real fractal systems, however, do not extend to all space scale, but rather have a finite size. In such a case, the power law behavior of the scattered intensity disappears for low Q values, where the Guinier limit begins. Chen and Teixeira[64] proposed a structure factor suitable for describing a finite fractal aggregate constituted by m monomers, encompassing Gaussian and fractal behavior, with a cutoff correlation length ξ:

$$I(Q) \propto \frac{m \sin[(D_f - 1)\arctan(Q\xi)]}{(D_f - 1)Q\xi(1 + Q^2\xi^2)^{(D_f-1)/2}} \tag{8}$$

For a rigid rod with a small diameter compared to its length L, the form factor becomes

$$I(Q) \propto \frac{2}{QL}\int_0^{QL}\frac{\sin(x)}{x}\,dx - \left(\frac{2}{QL}\sin\left(\frac{QL}{2}\right)\right)^2 \tag{9}$$

In the case of a long rod ($QL \gg 1$), eq 9 becomes $I(Q) \propto Q^{-1}$.

Results and Discussion

In the most diluted solutions, aggregation is triggered by increasing ionic strength; the role of the added ions is to shield the charged sulfonate groups on the porphyrins allowing for a closer approach of molecules to occur. In the absence of salt, aggregation is fostered by increasing porphyrin concentration.

The structural and dynamical properties of the resulting aggregates have been investigated by light-scattering experiments. A comparison between the intensity profiles at different concentrations, shown in Figure 2, suggests that salt-induced aggregates have bigger size, while, in the absence of salt, the size of the aggregates decreases with increasing porphyrin concentration.

The light scattered by the aggregates is depolarized, the depolarization ratio ($P = G_{VH}(\mathbf{Q}, 0)/I(Q) = 1/15\ \beta^2/\alpha^2$) being about 0.08. The anisotropy in the polarizability tensor derives from the strong exciton coupling between porphyrins, and it is almost independent of concentration (at least in the investigated range).

In the presence of salt, from the autocorrelation function relaxation rate of the most diluted solution in polarized and depolarized configuration, no difference is evident, as is shown in Figure 3. This finding indicates that rotational motions do not contribute to the width of the quasielastic optical spectrum. Indeed, although aggregate building blocks are optically anisotropic, the rotational diffusion of the whole aggregate is too

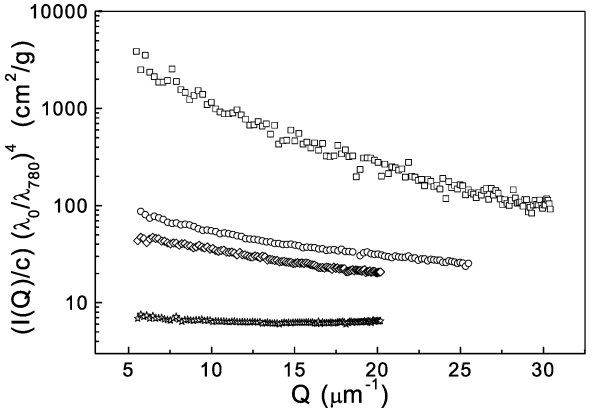

Figure 2. Intensity profile normalized by porphyrin concentration and corrected for the wavelength: $c_{TPPS} = 3\ \mu$M (squares) in the presence of NaCl (1.5 M), 40 μM (circles), 250 μM (diamonds), and 500 μM (stars); all at pH = 2.7.

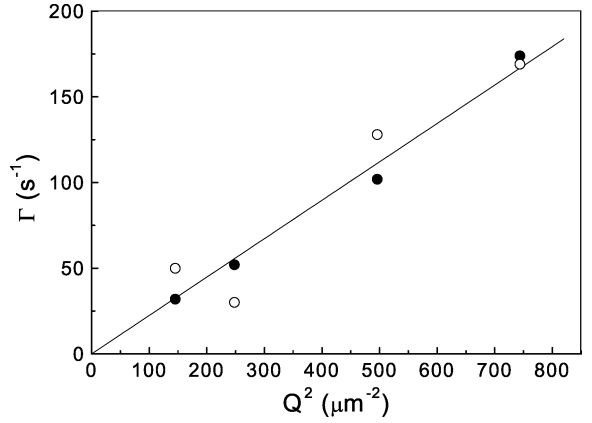

Figure 3. Relaxation rate of the depolarized (hollow circles) and polarized (filled circles) correlation function at different scattering angles for a 3 μM porphyrin solution in the presence of NaCl (1.5 M).

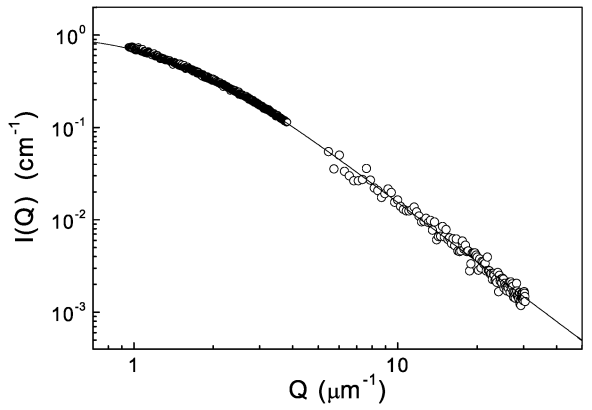

Figure 4. Elastic light scattering intensity profile at small and wide angles for the same solution as in Figure 3 ($\lambda_0 = 532$ nm). The continuous line is the fit according to the Chen−Teixeira equation.

slow to be detected. In other words, Θ is so small that eqs 3 and 4 are not distinguishable from each other.

This result can be understood considering the large size of the aggregates and their internal rigidity: the diffusion coefficient extracted from the slope of the linear Q^2 dependence of the relaxation rate, $D = 2.5 \times 10^{-9}$ cm^2/s, gives, for the aggregate, a mean hydrodynamic radius $R_H = 0.85 \pm 0.05\ \mu$m.

To check the form and structure of these aggregates, the intensity profile (see Figure 4) has been measured as a combination of SLS data at wide and small angles (SALS). A typical fractal profile, which obeys the Chen−Teixeira relation,

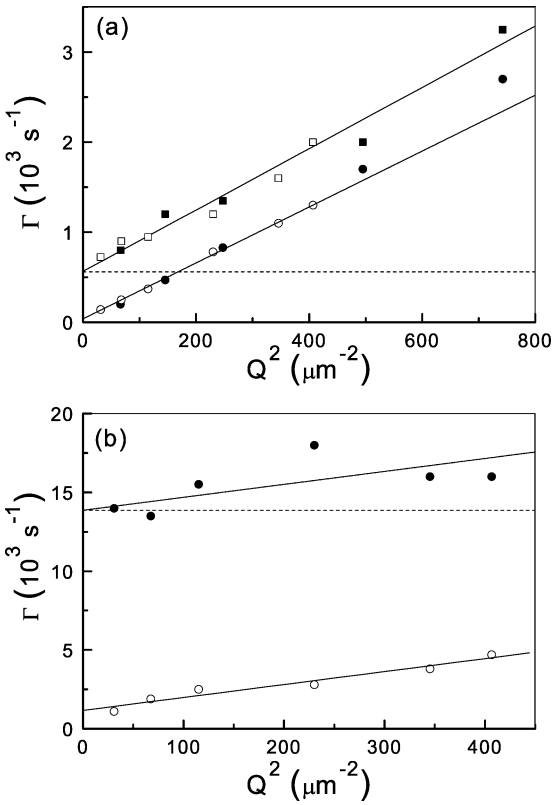

Figure 5. (a) Relaxation rates of the depolarized (squares) and polarized (circles) correlation function at different scattering angles for $c_{TPPS} = 40\ \mu$M (filled symbols) and for $c_{TPPS} = 250\ \mu$M (open symbols). The straight lines are the fit result in the region $Q^2 \leq 400$ 1/μm^2. (b) Relaxation rates of the depolarized (filled circles) and polarized (open circles) correlation function at different scattering angles for the solution at $c_{TPPS} = 500\ \mu$M. The dashed line represents the value of the depolarized relaxation rate at $Q \rightarrow 0$.

is obtained. The fit procedure using eq 8 gives $D_f = 2.2 \pm 0.1$ for the fractal dimension and $\xi = 0.7 \pm 0.1\ \mu$m for the cutoff length (the bending region of the curve). From this latter quantity, the radius of gyration can be determined: $R_g = \sqrt{3}\xi \approx 1.2\ \mu$m. The ratio $\beta = R_H/R_g$ measures the porosity of the aggregate, and the obtained value of $\approx$0.7 is in good agreement with that expected for fractals with an exponential cutoff in the density correlation function ($\beta = 0.62$).[65,66]

The value of the fractal dimension (consistent with that found in a previous work[41] for an analogous system) suggests that an RLA (reaction-limited aggregation) mechanism is driving the aggregation process ($D_f = 2.1$). Recently, some authors[67] showed that the measured fractal dimension of a DLCCA ($D_f = 1.75$) and an RLCA (reaction-limited cluster−cluster aggregation; $D_f = 2.1$) aggregate is an increasing function of the monomer aspect ratio. In particular, aggregation of rod-shaped building blocks leads to a loss of distinction between the two kinetic mechanisms of growth as the axial asymmetry increases. Thus, the value of 2.2 obtained for the fractal dimension could be also due to a nonspherical shape of the fractal building blocks.

In the absence of salt, aggregation is fostered by an increasing concentration of porphyrin; in this case, a significant structural change occurs, as evidenced by the polarized and the depolarized autocorrelation functions and by the intensity profile.

Figure 5a shows that, in the concentration range from 40 up to 250 μM, in the depolarized configuration, the relaxation rate approaches a finite value for $Q \rightarrow 0$, giving the value $\Theta \approx 95$ 1/s for the rotational diffusion coefficient. The slope of the linear dependence of both the polarized and the depolarized relaxation

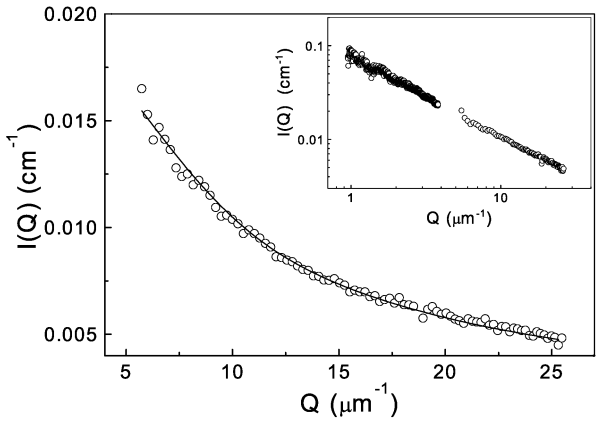

Figure 6. Elastic intensity profile at wide angle for the 40 μM porphyrin concentration ($\lambda_0 = 532$ nm). The continuous line is obtained by eq 9 with $L = 0.6$. The inset reports the small and wide angle scattering on a log−log scale.

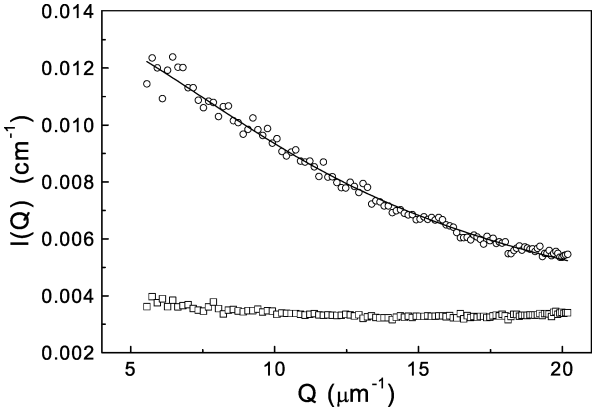

Figure 7. Elastic light scattering intensity profile ($\lambda_0 = 780$ nm) for the solutions at a 250 μM porphyrin concentration (circles) and at 500 μM (squares). The continuous line is the fit according to eq 9.

rate gives, as in the previous case, the translational diffusion coefficient, $D = 3.3 \times 10^{-8}$ cm^2/s.

In this case, the hydrodynamic radius cannot be evaluated by the Einstein−Stokes relation, which is valid for spherical aggregates. As for the fractal aggregates, shape and structure are obtained by measuring the scattered intensity profile, which is reported in the inset of Figure 6 for the solution at 40 μM as an example. In the entire investigated Q range, it displays a $Q^{-0.9}$ behavior (very close to the theoretical value of a long thin rod, −1), suggesting a rodlike assembling of porphyrins on a micrometric scale.

Assuming that aggegates have an ellipsoidal form and that the investigated concentration range lies in the dilute regime, the following Perrin's equations hold:[59]

$$\Theta = \frac{3k_BT}{16\pi\eta(L/2)^3}\frac{(2-\rho)G(\rho)-1}{(1-\rho^2)} \tag{10}$$

$$D = \frac{k_BT}{6\pi\eta(L/2)}G(\rho) \tag{11}$$

where $L/2$ and ρ are the major semiaxis and the axial ratio, respectively, and $G(\rho)$ for prolate ellipsoid ($\rho < 1$) has the form:

$$G(\rho) = (1-\rho^2)^{-1/2}\ln\left\{\frac{1+(1-\rho^2)^{1/2}}{\rho}\right\} \tag{12}$$

Equation 11 can be regarded as the Einstein−Stokes relation for the equivalent sphere of hydrodynamic radius $R_H = (L/2)/G(\rho)$. Solving both the Perrin's equations by using standard methods for nonlinear systems of equations with $L/2$ and ρ as unknown parameters and Θ and D as measured quantities, it follows that $L = 0.50 \pm 0.05$ μm and $\rho = 0.02 \pm 0.008$; the latter value indicates that aggregates are more likely to be very elongated cylinders.

The same values are obtained by applying the Broersma relations for the translational and rotational diffusion of a rigid rod:[59]

$$\Theta = \frac{3k_BT}{\pi\eta L^3}(\delta - \zeta) \tag{13}$$

$$D = \frac{k_BT}{3\pi\eta L}\left(\delta - \frac{1}{2}(\gamma_{||} + \gamma_\perp)\right) \tag{14}$$

with $D = (D_{||} + 2D_\perp)/3$, $D_{||} = (k_BT/2\pi\eta L)(\delta - \gamma_{||})$, $D_\perp = (k_BT/4\pi\eta L)(\delta - \gamma_\perp)$, and

$$\delta = \ln(2/\rho)$$

$$\zeta = 1.45 - 7.5(1/\delta - 0.27)^2$$

$$\gamma_{||} = 1.27 - 7.4(1/\delta - 0.34)^2$$

$$\gamma_\perp = 0.19 - 4.2(1/\delta - 0.39)^2$$

From the values of $D_{||}$ and $D_\perp$, it follows that the coupling parameter is $\gamma < 5$ (for $Q < 20$ μm^{-1}). Consequently, even if $QL > 3$, the contribution from translational and rotational coupling can be neglected so that eqs 3 and 4 represent a good approximation.

From the diffraction point of view, the minor semiaxis is not large enough for light scattered from two points along a cross-section diameter to produce a significant phase difference. As a consequence, the value of the minor axis resulting from the use of the ellipsoid form factor can have little meaning. Therefore, the use of the thin rigid rod form factor gives a more reproducible and meaningful value of the fitting parameters.

Data obtained by static and dynamic measurements suggest a significant size polydispersity; in the small angle region, the scattered intensity is mainly due to rods with micrometric length, whereas in the wide angle region submicrometric rods mainly contribute to the scattering. In fact, in the latter region, the form factor of a rod with length $L = 0.60$ μm (eq 9) agrees well with the experimental intensity profile, as shown in Figure 6, and with the dynamic scattering results.

Above $c_{TPPS} = 40$ μM, the scattered intensity at a small angle is very low (data not shown), suggesting that micrometric rods are absent. At these concentrations, the intensity profile does not follow the power law valid for $QL \gg 1$ and eq 9 allows for the estimate of L. Up to a 250 μM porphyrin concentration, the wide angle scattering profile gives for the rod length the value $L = 0.4 \pm 0.05$ μm (see Figure 7 and Table 1).

Both static and dynamic results give consistent values of the conformation and size of the aggregates; moreover, the dynamic measurements add information on the rod diameter, $\rho L \approx 10$ nm.

On further increasing porphyrin concentration up to 500 μM, the rotational diffusion coefficient of aggregates increases as well, as shown by the rate of the depolarized correlation function in Figure 5b that has the value of $\Theta \approx 2050$ 1/s, while the translational diffusion coefficient is $D = 8.2 \times 10^{-8}$ cm^2/s. Following the same procedure as described above and solving

TABLE 1: Rod Length Values at Different Porphyrin Concentrations[a]

c_{TPPS} (μM)	D (cm^2/s)	Θ (1/s)	L (μm)	ρ
40	3.3×10^{-8}	95	0.5 (>0.6)	0.02
100	3.5×10^{-8}	100	0.5 (0.4)	0.02
250	3.3×10^{-8}	95	0.5 (0.4)	0.02
500	8.2×10^{-8}	2050	0.2	0.02

[a] The values of the rod length in parentheses refer to the results obtained by the static light scattering experiments.

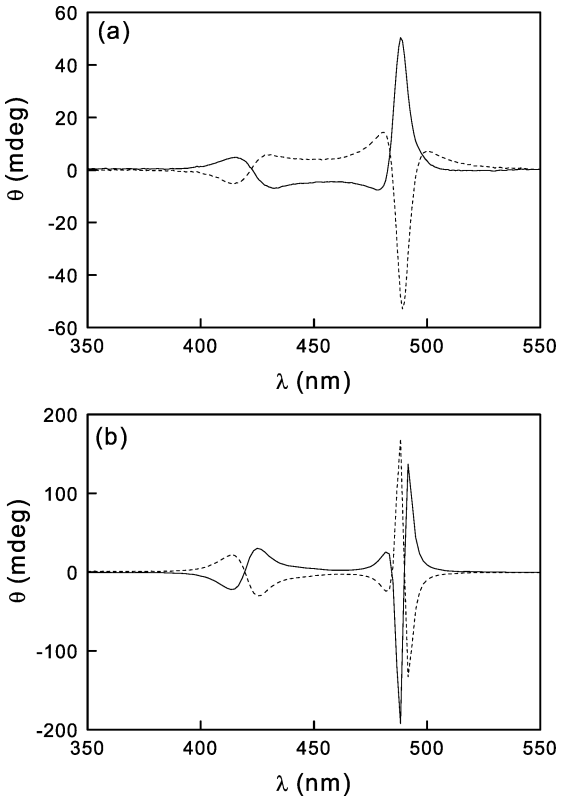

Figure 8. Induced circular dichroism bands for the solutions at (a) $c_{TPPS} = 3\ \mu$M with NaCl and (b) at $c_{TPPS} = 40\ \mu$M both in the presence of the D (solid line) and L (dashed line) form of the tartaric acid.

the Perrin's (or Broersma) equations, we get $L = 0.20 \pm 0.02$ μm. The diameter of the rod does not vary significantly on increasing concentration. In this case, the coupling parameter is $\gamma < 0.5$ (for $Q < 20$ 1/μm).

For this more concentrated solution, the small size of the rods does not allow for a significant diffraction pattern (see the flat intensity profile in Figure 7).

It is important to note that for all the investigated concentration values the condition $NL^3 < 1$ holds; this occurrence guarantees the validity of the hypothesis about the dilute regime of the solutions investigated.

A rodlike structure is consistent with a helical arrangement of porphyrin molecules in the J-aggregates for which the projection of the transition dipole moment is mostly perpendicular to the long axis of the rod,[4] as also observed for other J-aggregate wires.

To understand if the fractal-to-rod structural change has a local origin, the induced chirality by the template tartaric acid has been investigated. Figure 8 displays the induced circular dichroism (ICD) for the solutions containing different mesoscopic arrangements of porphyrins; the ICD appears in correspondence with the J-aggregate absorption bands (422 and 490 nm). The contribution from linear dichroism can be considered negligible as it is shown by the opposite sign of the spectra in the presence of the two opposite enantiomers.

Apart from the effect of the strong scattering contribution due to the fractal structure which broadens the ICD bands, the most relevant feature is that the spectra obtained for fractal aggregates are opposite with respect to those obtained for rod-shaped aggregates. This result is rather surprising and indicates the occurrence of opposite chirality in the J-aggregates, depending on the presence of salt. A tentative explanation could be that this effect is due to the interaction potential between porphyrins. In fact, by considering that the high ionic strength screens the sulfonate groups of the porphyrins, the repulsive energy barrier between two porphyrins is lowered and their approach is consequently favored, allowing for an unconstrained local arrangement. In the absence of salt and at higher porphyrin concentration, most of the sulfonate groups are not screened and the local arrangement is forced by electrostatic repulsion. Therefore, the fractal-to-rod change is driven by the potential interaction between porphyrins, whereas concentration tunes the rod size.

Conclusions

The ability to control the size and shape of aggregates formed by self-assembly is fundamental for employing new materials in nanodevices. The results reported in this paper show that the mesoscopic structure of porphyrin J-aggregates in solution is not an intrinsic property of porphyrin itself; indeed, tuning properly both ionic strength and concentration represents an easy and efficient way to obtain aggregates having controlled size and shape.

The shielding of the repulsive potential between porphyrins on increasing ionic strength drives the formation of fractal J-aggregates even at low porphyrin concentration. On the contrary, at low ionic strength, in the absence of added salt and at higher porphyrin concentration, a structural change to rod-shaped J-aggregates occurs.

The use of a chiral template, inducing chirality on the J-aggregates, seems to indicate that the structural difference between fractal and rod-shaped aggregates occurs locally and not only at the mesoscopic scale. In particular, acting on the chirality of the aggregates could allow for the development and improvement of photoconductive nanorods[68] sensitive to circularly polarized light.

Upon further increasing porphyrin concentration (at the same low ionic strength), J-aggregates maintain the rod-shaped geometry and about the same diameter but they are significantly shorter. This occurrence can be due to the fact that a large number of shorter rods gives rise to a lower steric hindrance with respect to a small number of longer rods.

The observed decrease of the rod length with increasing concentration is in line with X-ray results reported by some authors[26] on an analogous system. In this latter case, porphyrins are arranged in even shorter rods at concentration values 10 times higher (and even more) than those used in our investigation.

References and Notes

(1) Lidzey, D. G.; Bradley, D. D. C.; Armitage, A.; Walker, S.; Skolnick, M. S. *Science* **2000**, *288*, 1620.

(2) Chakrabarti, A.; Schmidt, A.; Valencia, V.; Fluegel, B.; Mazumdar, S.; Armstrong, N.; Peyghambarian, N. *Phys. Rev. B* **1998**, *57*, R4206.

(3) Van der Boom, T.; Hayes, R. T.; Zhao, Y.; Bushard, P. J.; Weiss, E. A.; Wasielewski, M. R. *J. Am. Chem. Soc.* **2002**, *124*, 9582.

(4) Lagoudakis, P. G.; de Souza, M. M.; Schindler, F.; Lupton, J. M.; Feldmann, J.; Wenus, J.; Lidzey, D. G. *Phys. Rev. Lett.* **2004**, *93*, 257401.

(5) Li, G.; Fudickar, W.; Skupin, M.; Klyszcz, A.; Draeger, C.; Lauer, M.; Fuhrhop, J.-H. *Angew. Chem., Int. Ed.* **2002**, *41*, 1828.
(6) Li, L.-L.; Yang, C.-J.; Chen, W.-H.; Lin, K.-J. *Angew. Chem., Int. Ed.* **2003**, *42*, 1505.
(7) Sayama, K.; Tsukagoshi, S.; Hara, K.; Ohga, Y.; Shinpou, A.; Abe, Y.; Suga, S.; Arakawa, H. *J. Phys. Chem. B* **2002**, *106*, 1363.
(8) Daniel, C.; Herz, L. M.; Silva, C.; Hoeben, F. J. M.; Jonkheijm, P.; Schenning, A. P. H. J.; Meijer, E. W. *Phys. Rev. B* **2003**, *68*, 235212.
(9) Herz, L. M.; Daniel, C.; Silva, C.; Hoeben, F. J. M.; Schenning, A. P. H. J.; Meijer, E. W.; Friend, R. H.; Phillips, R. T. *Phys. Rev. B* **2003**, *68*, 45203.
(10) Pasternack, R. F.; Gibbs, E. *J. Met. Ions Biol. Syst.* **1996**, *33*, 367.
(11) Schwab, A. D.; Smith, D. E.; Rich, C. S.; Young, E. R.; Smith, W. F.; de Paula, J. C. *J. Phys. Chem. B* **2003**, *107*, 11339.
(12) Koti, A. S.; Periasamy, N. *Chem. Mater.* **2003**, *15*, 369.
(13) Lauceri, R.; Raudino, A.; Monsù Scolaro, L.; Micali, N.; Purrello, R. *J. Am. Chem. Soc.* **2002**, *124*, 894.
(14) Bellacchio, E.; Lauceri, R.; Gurrieri, S.; Monsù Scolaro, L.; Romeo, A.; Purrello, R. *J. Am. Chem. Soc.* **1998**, *120*, 12353.
(15) Ohno, O.; Kaizu, Y.; Kobayashi, H. *J. Chem. Phys.* **1993**, *99*, 4128.
(16) Pasternack, R. F.; Schaefer, K. F.; Hambright, P. *Inorg. Chem.* **1994**, *33*, 2062.
(17) Ribo, J. M.; Crusats, J.; Farrera, J. A.; Valero, M. L. *J. Chem. Soc., Chem. Commun.* **1994**, 681.
(18) Akins, D. L.; Ozcelik, S.; Zhu, H. R.; Guo, C. *J. Phys. Chem.* **1996**, *100*, 14390.
(19) Akins, D. L.; Zhu, H. R.; Guo, C. *J. Phys. Chem.* **1996**, *100*, 5420.
(20) Guo, C.; Ren, B.; Akins, D. L. *J. Phys. Chem. B* **1998**, *102*, 8751.
(21) Collings, P. J.; Gibbs, E. J.; Starr, T. E.; Vafek, O.; Yee, C.; Pomerance, L. A.; Pasternack, R. F. *J. Phys. Chem. B* **1999**, *103*, 8474.
(22) Rubires, R.; Crusats, J.; El-Hachemi, Z.; Jaramillo, T.; Lopez, M.; Valls, E.; Farrera, J. A.; Ribo, J. M. *New J. Chem.* **1999**, *23*, 189.
(23) Ren, B.; Tian, Z. Q.; Guo, C.; Akins, D. L. *Chem. Phys. Lett.* **2000**, *328*, 17.
(24) Ribo, J. M.; Crusats, J.; Sagues, F.; Claret, J.; Rubires, R. *Science* **2001**, *292*, 2063.
(25) Rubires, R.; Muller, C.; Campos, L.; El-Hachemi, Z.; Pakhomov, G. L.; Ribo, J. M. *J. Porphyr. Phthalocyanines* **2002**, *6*, 107.
(26) Gandini, S. C. M.; Gelamo, E. L.; Itri, R.; Tabak, M. *Biophys. J.* **2003**, *85*, 1259.
(27) Lauceri, R.; Gurrieri, S.; Bellacchio, E.; Contino, A.; Scolaro, L. M.; Romeo, A.; Toscano, A.; Purrello, R. *Supramol. Chem.* **2000**, *12*, 193.
(28) Micali, N.; Romeo, A.; Lauceri, R.; Purrello, R.; Mallamace, F.; Scolaro, L. M. *J. Phys. Chem. B* **2000**, *104*, 9416.
(29) Purrello, R.; Scolaro, L. M.; Bellacchio, E.; Gurrieri, S.; Romeo, A. *Inorg. Chem.* **1998**, *37*, 3647.
(30) Purrello, R.; Bellacchio, E.; Gurrieri, S.; Lauceri, R.; Raudino, A.; Scolaro, L. M.; Santoro, A. M. *J. Phys. Chem. B* **1998**, *102*, 8852.
(31) Paulo, P. M. R.; Gronheid, R.; De Schryver, F. C.; Costa, S. M. B. *Macromolecules* **2003**, *36*, 9135.
(32) Paulo, P. M. R.; Costa, S. M. B. *Photochem. Photobiol. Sci.* **2003**, *2*, 597.
(33) Gandini, S. C. M.; Yushmanov, V. E.; Borissevitch, I. E.; Tabak, M. *Langmuir* **1999**, *15*, 6233.
(34) Maiti, N. C.; Mazumdar, S.; Periasamy, N. *J. Porphyr. Phthalocyanines* **1998**, *2*, 369.
(35) Maiti, N. C.; Mazumdar, S.; Periasamy, N. *J. Phys. Chem. B* **1998**, *102*, 1528.
(36) Jiang, S. G.; Liu, M. H. *J. Phys. Chem. B* **2004**, *108*, 2880.
(37) Zhang, L.; Yuan, J.; Liu, M. H. *J. Phys. Chem. B* **2003**, *107*, 12768.
(38) Castriciano, M. A.; Romeo, A.; Villari, V.; Micali, N.; Monsù Scolaro, L. *J. Phys. Chem. B* **2004**, *108*, 9054.
(39) Castriciano, M. A.; Romeo, A.; Villari, V.; Angelini, N.; Micali, N.; Scolaro, L. M. *J. Phys. Chem. B* **2005**, *109*, 12086.
(40) Andrade, S. M.; Costa, S. M. B. *Chem.—Eur. J.* **2006**, *12*, 1046.
(41) Micali, N.; Mallamace, F.; Romeo, A.; Purrello, R.; Monsù Scolaro, L. *J. Phys. Chem. B* **2000**, *104*, 5897.
(42) Castriciano, M. A.; Romeo, A.; Villari, V.; Micali, N.; Monsù Scolaro, L. *J. Phys. Chem. B* **2003**, *107*, 8765.
(43) Rotomskis, R.; Augulis, R.; Snitka, V.; Valiokas, R.; Liedberg, B. *J. Phys. Chem. B* **2004**, *108*, 2833.
(44) Markel, V. A.; Shalaev, V. M.; Stechel, E. B.; Kim, W.; Armstrong, R. L. *Phys. Rev. B* **1996**, *53*, 2425.
(45) Shalaev, V. M.; Poliakov, E. Y.; Markel, V. A. *Phys. Rev. B* **1996**, *53*, 2437.
(46) Monsù Scolaro, L.; Romeo, A.; Castriciano, M. A.; Micali, N. *Chem. Commun.* **2005**, *24*, 3018.
(47) Kano, H.; Saito, T.; Kobayashi, T. *J. Phys. Chem. B* **2001**, *105*, 413.
(48) Kano, H.; Saito, T.; Kobayashi, T. *J. Phys. Chem. A* **2002**, *106*, 3445.
(49) Kano, H.; Kobayashi, T. *J. Chem. Phys.* **2002**, *116*, 184.
(50) Collini, E.; Ferrante, C.; Bozio, R. *J. Phys. Chem. B* **2005**, *109*, 2.
(51) Micali, N.; Villari, V.; Monsù Scolaro, L.; Romeo, A.; Castriciano, M. A. *Phys. Rev. E* **2005**, *72*, 50401R.
(52) Parkash, J.; Robblee, J. H.; Agnew, J.; Gibbs, E.; Collings, P.; Pasternack, R. F.; de Paula, J. C. *Biophys. J.* **1998**, *74*, 2089.
(53) Piazza, R.; Degiorgio, V.; Corti, M.; Stavans, J. *Phys. Rev. B* **1990**, *42*, R4885.
(54) De Souza Lima, M. M.; Wong, J. T.; Paillet, M.; Borsali, R.; Pecora, R. *Langmuir* **2003**, *19*, 24.
(55) Berne, B. J.; Pecora, R. *Dynamic Light Scattering with Applications to chemistry, biology and physics*; John Wiley and Sons inc.: New York, 1976.
(56) Provencher, S. W. *Comput. Phys. Commun.* **1982**, *27*, 229.
(57) Maeda, T.; Fujime, S. *Macromolecules* **1983**, *17*, 1157.
(58) Zero, K. M.; Pecora, R. *Macromolecules* **1982**, *15*, 87.
(59) Zero, K.; Pecora, R. Application of Photon Correlation Spectroscopy. In *Dinamic Light Scattering*; Pecora, R., Ed.; Plenum Press: New York, 1985; p 59.
(60) Russo, P. S. The Method and Some Applications. In *Dinamic Light Scattering*; Brown, W., Ed.; Clarendon Press: Oxford, 1996; p 512.
(61) Cush, R.; Dorman, D.; Russo, P. *Macromolecules* **2004**, *37*, 9577.
(62) Stanley, H. E., Ostrowsky, N., Eds. *On Growth and Form*; NATO ASI Series; Martinus Nijhoff Publishers: Dordrecht, 1986.
(63) Mallamace, F.; Micali, N.; Trusso, S.; Monsù Scolaro, L.; Romeo, A.; Terracina, A. *Phys. Rev. Lett.* **1996**, *76*, 4741.
(64) Chen, S. H.; Teixeira, J. *Phys. Rev. Lett.* **1986**, *57*, 2583.
(65) Pusey, P. N.; Rarity, J. G.; Klein, R.; Weitz, D. A. *Phys. Rev. Lett.* **1987**, *59*, 2122.
(66) Wiltzius, P. *Phys. Rev. Lett.* **1987**, *58*, 710.
(67) Mohraz, A.; Moler, D. B.; Ziff, R. M.; Solomon, M. J. *Phys. Rev. Lett.* **2004**, *92*, 155503-1.
(68) Schwab, A. D.; Smith, D. E.; Bond-Watts, B.; Johnston, D. E.; Hone, J.; Johnson, A. T.; de Paula, J. C.; Smith, W. F. *Nano Lett.* **2004**, *4*, 1261.